down on greater slopes, the deposits could eventually become even steeper because the internal tidal energy decreases with increasing seafloor gradient above the critical angle. Other processes are at work in shaping continental slopes, and at least one of these, turbidity currents, also has the potential to be an important cause for the relative flatness of continental slopes (*20*).

References and Notes

1. L. F. Pratson, W. F. Haxby, *Geology* **24**, 3 (1996).
2. D. O'Grady, J. Syvitski, L. F. Pratson, J. F. Sarg, *Geology* **28**, 207 (2000).
3. O. M. Phillips, *The Dynamics of the Upper Ocean* (Cambridge Univ. Press, London, 1977).
4. S. J. Prinsenberg, W. Wilmot, M. Rattray Jr., *Deep-Sea Res.* **16**, 179 (1974).
5. D. A. Cacchione, L. Pratson, A. Ogston, paper presented at the Ocean Sciences Meeting of the American Society of Limnology and Oceanography and the American Geophysical Union, San Antonio, TX, 24 to 28 January 2000.
6. Long-term studies of sediment processes and the formation of stratigraphic sequences were carried out on the continental terraces off New Jersey and northern California during the U.S. Office of Naval Research (ONR) STRATAFORM program from 1995 to 1999. The continental slopes in these two regions have different regional gradients (4° in New Jersey versus 2° in northern California) and different geology (e.g., New Jersey is a passive margin and northern California is an active margin).
7. L. Pratson *et al.*, *Eos* **80**, 37 (1999).
8. M. E. Conkright *et al.*, *Nat. Ocean. Data Ctr. Int. Rep. 14* (1999).
9. F. Hotchkiss, C. I. Wunsch, *Deep-Sea Res.* **29**, 415 (1982).
10. D. A. Cacchione, C. I. Wunsch, *J. Fluid Mech.* **66**, 223 (1974).
11. J. Ribbe, P. Holloway, *Cont. Shelf Res.* **21**, 395 (2001).
12. O. Zikanov, D. N. Slinn, *J. Fluid Mech.* **445**, 235 (2001).
13. I. N. McCave, in *Shelf Sediment Transport: Process and Pattern*, D. Swift, D. Duane, O. Pilkey, Eds. (Dowden, Hutchinson, and Ross, Stroudsburg, PA, 1972), chap. 10.
14. R. J. S. Whitehouse, R. L. Soulsby, W. Roberts, H. J. Mitchener, *Dynamics of Estuarine Muds* (Report SR 527, HR Wallingford Ltd., Wallingford, UK, 1999).
15. G. N. Ivey, K. B. Winters, I. P. D. DeSilva, *J. Fluid Mech.* **418**, 59 (2000).
16. J. S. Turner, *Buoyancy Effects in Fluids* (Cambridge Univ. Press, Cambridge, ed. 1, 1973), pp. 128–130.
17. R. R. Dickson, I. N. McCave, *Deep-Sea Res.* **33**, 791 (1986).
18. E. E. McPhee, thesis, University of Washington, Seattle (2000).
19. C. R. Alexander, A. M. Simoneau, *Mar. Geol.* **154**, 243 (1999).
20. G. Parker, S. Kostic, J. Marr, *J. Sed. Res.*, in press.

21. We thank the ONR Marine Geology and Geophysics Program and J. Kravitz for supporting this work in STRATAFORM. Additional support came from ONR Physical Oceanography and U.S. Geological Survey's Coastal and Marine Program.

14 January 2002; accepted 21 March 2002

Global Cooling After the Eruption of Mount Pinatubo: A Test of Climate Feedback by Water Vapor

Brian J. Soden,[1]* Richard T. Wetherald,[1] Georgiy L. Stenchikov,[2] Alan Robock[2]

The sensitivity of Earth's climate to an external radiative forcing depends critically on the response of water vapor. We use the global cooling and drying of the atmosphere that was observed after the eruption of Mount Pinatubo to test model predictions of the climate feedback from water vapor. Here, we first highlight the success of the model in reproducing the observed drying after the volcanic eruption. Then, by comparing model simulations with and without water vapor feedback, we demonstrate the importance of the atmospheric drying in amplifying the temperature change and show that, without the strong positive feedback from water vapor, the model is unable to reproduce the observed cooling. These results provide quantitative evidence of the reliability of water vapor feedback in current climate models, which is crucial to their use for global warming projections.

Water vapor plays a key role in regulating Earth's climate. It is the dominant greenhouse gas (*1*) and provides the largest known feedback mechanism for amplifying climate change (*2*). Because the equilibrium vapor pressure of water increases rapidly with temperature, it is generally believed that the concentration of water vapor will rise as the atmosphere warms. If so, the added radiative absorption from water vapor will act to further amplify the initial warming. Current climate models suggest that this provides an important positive feedback, roughly doubling the sensitivity of the surface temperature to an increase in anthropogenic greenhouse gases (*3–5*). If the actual feedback by water vapor is substantially weaker than predicted by current models, both the magnitude of warming and range of uncertainty resulting from a doubling of CO_2 would be substantially diminished (*5*).

Despite the importance of water vapor feedback in determining the sensitivity of Earth's climate, the fidelity of its representation in climate models has remained a topic of debate for more than a decade (*6*, *7*). The difficulty in verifying models partly stems from the lack of observed climate variations that can provide quantitative tests of the feedbacks in question. Assessments of water vapor feedback are often based on regional, seasonal, or interannual variations of Earth's climate (*8–12*), which differ markedly in both cause and character from the more uniform, radiatively forced perturbations that result from increasing CO_2. Thus, their conclusions are often qualitative, and their relevance to feedbacks that arise from global warming are often questioned (*6*, *13–15*).

It has long been recognized that volcanic eruptions provide a valuable opportunity to observe the climate system's response, albeit a transient one, to the presence of an external radiative forcing (*16–19*). Strong volcanic eruptions inject large amounts of sulfuric gas into the lower stratosphere where it combines with water and oxygen to form small, yet optically important, aerosol particles. Winds rapidly disperse the particles throughout the lower stratosphere, resulting in a near-global perturbation to the radiative energy balance. Because they are more effective at scattering sunlight than absorbing longwave terrestrial radiation, the net radiative effect of volcanic aerosols is to cool the planet.

The eruption of Mount Pinatubo in the Philippines in June of 1991 resulted in unprecedented observations of both radiative forcing from volcanic aerosols as well as the climate system's response to this forcing. Satellite observations confirm the decrease in solar heating due to Mount Pinatubo aerosols (*20–22*), which led to a global cooling of the lower troposphere (*23*, *24*). Associated with this cooling was a reduction in the global water vapor concentrations, which closely tracked the decrease in temperature (*25*). Thus, Mount Pinatubo provides a unique opportunity to not only study the sensitivity of the climate system but, more importantly, to also assess the response of water vapor and quantify its role in determining that sensitivity.

It is widely recognized that current climate models possess a strong positive feedback by water vapor (*3–5*, *26*). Nevertheless, one can

[1]Geophysical Fluid Dynamics Laboratory/National Oceanic and Atmospheric Administration, Princeton University, Princeton, NJ 08542, USA. [2]Department of Environmental Sciences, Rutgers University, New Brunswick, NJ 08901, USA.

*To whom correspondence should be addressed. E-mail: bjs@gfdl.gov

construct a model with a substantially weakened water vapor feedback by artificially removing the longwave (LW) (terrestrial) component of the feedback loop (*27*). Studies have shown that when water vapor feedback is removed in this fashion, the variability of the model is suppressed at all time scales, not just the longer (decadal to century) time scales associated with global warming. As we show, this enables us to evaluate model simulations with vastly differing strengths of water vapor feedback against observations of the actual climate system's response to the transient perturbation from Mount Pinatubo.

The model used here is an atmospheric general circulation model (GCM) with specified clouds coupled to a mixed-layer ocean with prescribed horizontal heat transports (*26*, *28*). Three pairs of model integrations are performed, each starting in January of 1991 (5 months before the eruption) and lasting 5 years. Each experiment pair consists of a "control" simulation, in which no aerosols are used, and a "Mount Pinatubo" simulation, in which the model is perturbed using the observed zonal-mean distribution of Mount Pinatubo aerosols (*26*, *29*).

Because the transient response of the model depends on both its sensitivity and the external radiative forcing imposed on it, we first demonstrate the consistency between the model-simulated radiative forcing with that measured by satellites (Fig. 1). Both the observations and model simulations yield very similar reductions in the absorbed solar or shortwave (SW) radiation (*30*), which are nearly twice as large as the reduction in emitted LW radiation, a net loss of radiative energy that cools the surface and lower troposphere.

The magnitude of this cooling is documented by satellite measurements of lower tropospheric temperature from the microwave sounding unit (MSU) (*31*). The MSU data indicate a peak global cooling of ~0.5 K nearly 18 months after the eruption, after which the temperature slowly returns to pre-Pinatubo levels (Fig. 2, top). In all three members of the ensemble, both the magnitude and duration of the model-predicted cooling agrees remarkably well with that measured by the MSU, confirming the model's ability to accurately reproduce the observed cooling (*32*).

Other sources of climate variability, most notably the El Niño–Southern Oscillation (ENSO), are not included in these model simulations but do influence the observed global temperature record. Indeed, the actual climate system was experiencing an extended El Niño during much of the early 1990s. However, because the observed anomalies are expressed relative to the pre-eruption value (*24*), and because this El Niño began before the eruption and was unusually persistent in nature, its impact on the global temperature anomalies from 1991 to 1995 is small. As evidence of this, Fig. 2 also shows the observed anomalies after being adjusted to remove the effects of ENSO (*33*). Removing ENSO slightly increases the peak cooling during mid-1992 and reduces the sharp drop in temperature at the end of 1995, both of which bring the observations and model simulations into better agreement.

How does the water vapor field respond to the radiatively forced cooling? The model-predicted anomalies in total column water vapor (Fig. 2, middle) indicate a distinct drying of the global atmosphere that agrees well with observations from the NASA Water Vapor Project (NVAP) (*25*). Both indicate a peak reduction in global water vapor of ~0.75 mm (~3%), which coincides with the period of maximum cooling (~0.5 K). The rate of global-mean drying (~6%/K) agrees with the rate at which the saturation vapor pressure decreases with temperature in the lower troposphere, implying a nearly constant relative humidity change in water vapor mass. Such behavior at the global scale is a widely recognized characteristic of climate models (*3*–*5*, *7*, *8*).

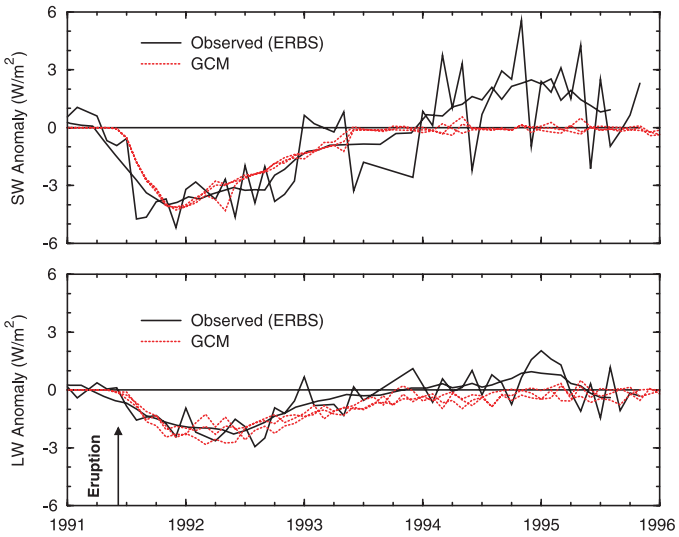

Fig. 1. Comparison of the observed anomalies in absorbed SW (top) and emitted LW (bottom) radiative fluxes at the top of the atmosphere from Earth Radiation Budget Satellite observations (black) and three ensembles of GCM simulations (red). The observed anomalies are expressed relative to a 1984 to 1990 base climatology, and the linear trend is removed (*30*). The results are expressed relative to the pre-eruption (January to May 1991) value of the anomaly and smoothed with a 7-month running mean (thick line). The GCM anomalies are computed as the difference between the control and Mount Pinatubo simulations for each ensemble member. Both the model and observed global averages are from 60N-60S due to the restriction of observed data to these latitudes.

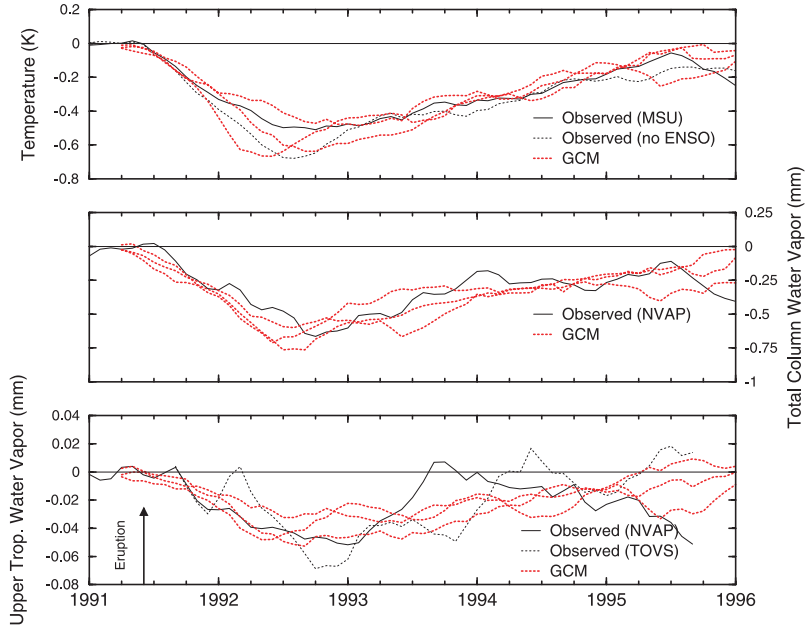

Fig. 2. Comparison of the observed (solid line) and model-predicted (dashed line) global-mean (90°N–90°S) changes in lower tropospheric temperature (**top**), total column water vapor (**middle**), and upper tropospheric (300 to 500 hPa) water vapor (**bottom**) after the eruption of Mount Pinatubo. The observed anomalies are computed using a 1979 to 1990 base climatology and expressed relative to the pre-eruption value, defined here as the mean anomaly for January 1991 to May 1991. The model anomalies are computed for each ensemble pair as the difference between the control and Mount Pinatubo experiments. All time series have been smoothed using a 7-month running mean.

Because the concentration of water vapor mass decreases roughly exponentially with height, changes in the total column water vapor are dominated by the response of water vapor in the lower troposphere. Yet, water vapor in the upper troposphere has a disproportionately large effect on the outgoing LW radiation (*34*) and, consequently, on climate sensitivity (*5*). Therefore, we also examine the response of the upper tropospheric water vapor between 300 and 500 hPa. Because retrievals of upper tropospheric water vapor are less reliable than those for the total column, we include both NVAP (*25*) and TIROS (Television Infrared Observation Satellite) Operational Vertical Sounder (TOVS) products (*26*, *35*) in our comparison (Fig. 2, bottom).

Both sets of observations indicate a drying of the upper troposphere after the Mount Pinatubo eruption, although TOVS suggests a somewhat larger drying than does NVAP. The model simulations show similar reductions during the first half of the record, where the cooling is greatest. After mid-1993, the NVAP anomalies rapidly return to pre-eruption levels, whereas the model simulations and the TOVS retrievals show a more gradual return. However, given the difficulty in retrieving such small concentrations of water vapor, it is unclear whether this discrepancy reflects a deficiency in the model or in the inversion algorithms used by NVAP.

This uncertainty can be avoided by comparing the model simulations directly with the satellite-observed radiances, thereby eliminating errors associated with the retrieval process (*36*). Figure 3 compares the satellite-observed equivalent blackbody temperatures at 6.7 μm ($T_{6.7}$) from the TOVS instrument (*37*) with those computed offline from the model's temperature and moisture profiles (*38*). Under clear skies, the 6.7-μm channel is primarily sensitive to changes in relative humidity averaged over a deep layer of the upper troposphere (roughly 200 to 500 hPa) (*39*). Thus, if the water vapor mass in the upper troposphere decreases by conserving relative humidity as the atmosphere cools, only a small perturbation to $T_{6.7}$ would be expected.

Figure 3 confirms that both the observations and model simulations yield only a modest reduction in $T_{6.7}$. In fact, the model-simulated anomalies are nearly identical to those obtained if one repeats the calculation of $T_{6.7}$ under the assumption of a constant relative humidity change in the model's water vapor field [shown as a green curve in Fig. 3 (*40*)]. In contrast, consider the anomalies in $T_{6.7}$ that would result if there was no decrease in water vapor mass in the model's upper troposphere [shown as a red curve in Fig. 3 (*41*)]. In this case, the $T_{6.7}$ would decrease by ~0.8 K, more than twice what was observed, due to a reduction in Planck emission (cooling) without a compensating reduction in atmospheric opacity (drying). Thus, without a nearly constant-relative-humidity drying of the upper troposphere, the model would be unable to reproduce the observed record of $T_{6.7}$.

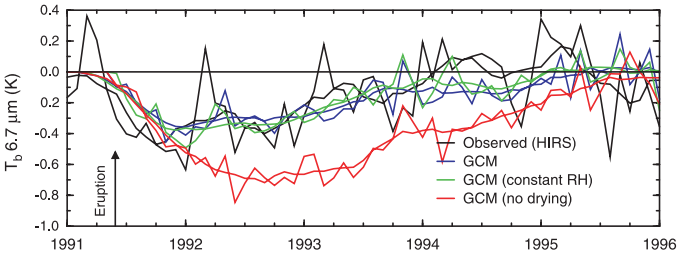

Fig. 3. Comparison of the observed (black) and GCM-simulated (blue) changes in global-mean (90°N–90°S) 6.7 μm brightness temperature ($T_{6.7}$). The observed anomalies are computed with respect to a 1979 to 1990 base climatology and expressed relative to their pre-eruption (January to May 1991) value. The GCM-simulated anomalies are computed as the ensemble-mean difference (Pinatubo – control) from the three pairs of GCM simulations. The green curve depicts the GCM-simulated $T_{6.7}$ computed under the assumption of a constant relative humidity change. The red curve depicts the GCM-simulated $T_{6.7}$ computed under the assumption of a constant, seasonally varying water vapor mixing ratio (i.e., no drying of the upper troposphere). The thick lines depict the 7-month running mean of each time series.

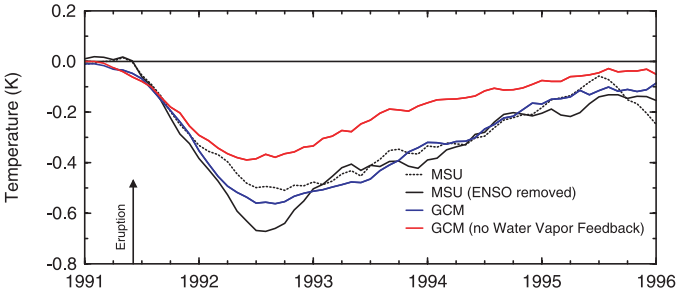

Fig. 4. Comparison of the satellite-observed (black) and model-predicted change in global-mean (90°N–90°S) lower tropospheric temperature for the standard GCM (blue) and the GCM without water vapor feedback (red). The observations are identical to those shown in Fig. 2. For clarity, we present only the ensemble-mean difference from each model of the three experiment pairs (Pinatubo – control). All curves are 7-month running means.

The above simulations show that the model atmosphere dries in response to the radiatively induced cooling in agreement with the observations. But to what extent does this drying amplify the cooling? To answer this question, we repeat our experiments using a configuration of the model in which water vapor feedback has been artificially suppressed by removing the LW component of the feedback loop (*26*, *42*). Once again, three pairs of integrations are performed, where each pair consists of a control simulation and a Mount Pinatubo simulation using the same aerosol forcing as before.

Figure 4 compares the Mount Pinatubo–induced cooling from both the "standard" (i.e., with water vapor feedback) and "no water vapor feedback" configurations of the model. In contrast to the standard model, the model without water vapor feedback is unable to reproduce the observed cooling. Over the period of June 1991 to December 1995, the standard model predicts an average global cooling of 0.31 K, which compares favorably with the observed cooling of 0.30 K [0.33 ± 0.03K, with ENSO signal removed (*43*)]. Without water vapor feedback, the model-predicted cooling is only 0.19 K. Thus, feedback from water vapor amplifies the magnitude of global cooling by ~60%, which is in good agreement with the amplification predicted by climate models in response to a doubling of CO_2 (*3*) and with that derived from idealized calculations using a constant relative humidity approximation (*5*).

To reproduce the observed temperature record after the eruption of Mount Pinatubo, the model requires a strong positive feedback, equivalent in magnitude to that predicted for water vapor. Although it is possible that other processes, such as clouds, could act in place of water vapor to provide the strong positive feedback necessary to amplify the cooling, the observational evidence clearly indicates a reduction in water vapor that is consistent with the model predictions.

This study highlights the role of water vapor feedback in amplifying the global cooling after the eruption of Mount Pinatubo. We note, however, that Mount Pinatubo does not provide a perfect proxy for global warming, because the nature of the external radiative forcing obviously differs between the two. Nevertheless, the results described here provide key evidence of the reliability of water vapor feedback predicted by current climate models in response to a global perturbation in the radiative energy balance. Given the importance of water vapor feedback in determining climate sensitivity, such confirmation is essential to the use of these models for global warming projections.

References and Notes

1. J. Kiehl, K. Trenberth, *Bull Am. Meteorol. Soc.* **78**, 197 (1997).
2. U. Cubasch, R. Cess, in *Climate Change: The IPCC*

Scientific Assessment, J. T. Houghton *et al*., Eds. (Cambridge Univ. Press, Cambridge, 1990).
3. R. Wetherald, S. Manabe, *J. Atmos. Sci.* **45**, 1397 (1988).
4. R. Cess *et al*., *J. Geophys. Res.* **95**, 16601 (1989).
5. I. Held, B. Soden, *Annu. Rev. Energy Environ.* **25**, 441, (2000).
6. R. Lindzen, *Bull. Am. Meteorol. Soc.* **71**, 288 (1990).
7. R. E. Dickinson *et al*., in *Climate Change 1995: The Science of Climate Change*, J. T. Houghton *et al*., Eds. (Cambridge Univ. Press, Cambridge, 1996).
8. A. Raval, V. Ramathan, *Nature* **342**, 758 (1989).
9. F. Wentz, M. Schabel, *Nature* **403**, 414 (2000).
10. D. Rind *et al*., *Nature* **349**, 500 (1991).
11. A. Del Genio, W. Kovari, Y. Mao-Sung, *Geophys. Res. Lett.* **21**, 2701 (1994).
12. B. Soden, *J. Clim.* **10**, 1050 (1997).
13. S. Bony, J. Duvel, H. Le Treut, *Clim. Dyn.* **11**, 307 (1995).
14. K. Lau, C. Ho, M. Chou, *Geophys Res. Lett.* **23**, 2971 (1996).
15. A. Inamdar, V. Ramanthan, *J. Geophys. Res.* **103**, 32177 (1998).
16. B. Franklin, *Manchester Literary and Philosophical Society Memoirs and Proceedings*, **2**, 122 (1784) [Reprinted in *Weatherwise*, **35**, 262 (1982)].
17. A. Robock, *Rev. Geophys.* **38**, 191 (2000).
18. J. Hansen, A. Lacis, R. Ruedy, M. Sato, *Geophys. Res. Lett.* **19**, 215 (1992).
19. I. Kirchner *et al*., *J. Geophys. Res.* **104**, 19039 (1999).
20. L. Stowe, R. Carey, P. Pellegrino, *Geophys. Res. Lett.* **19**, 159 (1992).
21. C. Trepte, R. Veiga, M. McCormick, *J. Geophys. Res.* **98**, 18563 (1993).
22. P. Minnis *et al*., *Science* **259**, 1411 (1993).
23. A. Robock, J. Mao, *J. Clim.* **8**, 1086 (1992).
24. D. Parker, H. Wilson, J. Christy, C. Folland, *Int. J. Clim.* **16**, 487 (1996).
25. D. Randel *et al*., *Bull. Am. Meteorol. Soc.* **77**, 1233 (1996).
26. Supplemental material is available at *Science* Online at www.sciencemag.org/cgi/content/full/296/5568/727/DC1.
27. A. Hall, S. Manabe, *J. Clim.* **12**, 2327 (1999).
28. The atmospheric model is a global spectral model with rhomboidal truncation at 30 wave numbers and 14 vertical levels. Details regarding the model's numerical formulation and physical parameterizations may be found in (*26*). The thickness of the ocean mixed-layer varies regionally and is specified according to its observed annual-mean climatology (S. Levitus, *NOAA Prof. Paper* 13, 1982).
29. G. Stenchikov *et al*., *J. Geophys. Res.* **103,** 13837 (1998).
30. Beginning in 1994, additional anomalies in the satellite-observations of top-of-atmosphere absorbed solar radiation become evident, which are unrelated to the Mount Pinatubo eruption and therefore not reproduced in the model simulations. These anomalies are believed to stem from decadal-scale changes in the tropical circulation over the mid- to late 1990's [see J. Chen *et al*., *Science* **295**, 838 (2002); and B. A. Wielicki *et al*., *Science* **295,** 841 (2002], but their veracity remains the subject of debate. If real, their absence in the model simulations implies that discrepancies between the observed and model-simulated temperature anomalies, delayed ~ 1 to 2 years by the climate system's thermal inertia, may occur by the mid-1990s. We therefore limit our analysis to the 5-year period 1991–1995, where the observations and model simulations are responding to similar changes in radiative forcing and encompass virtually all of the observed climate response to Pinatubo.
31. J. Christy, R. Spencer, W. Braswell, *J. Atmos. Oceanic Tech.* **17**, 1153 (2000).
32. A static, global weighting function is used to compute the equivalent lower tropospheric temperatures (2LT) from the model-simulated temperature profiles. See (*44*).
33. B. Santer *et al*., *J. Geophys. Res.* **106**, 28033 (2001).
34. P. Udelhofen, D. Hartmann, *J. Geophys. Res.* **100**, 7423 (1995).
35. J. Susskind *et al*., *Bull. Am. Meteorol. Soc.* **78**, 1449 (1997).
36. C. Rodgers, *Rev. Geophys. Space Phys.* **14**, 609 (1976).
37. We use intercalibrated, cloud-cleared radiances from the TOVS Radiance Pathfinder Project (*45*).
38. The "GCM-predicted" $T_{6.7}$ was computed offline by inserting the GCM profiles of temperature, water vapor mixing ratio, and Mount Pinatubo aerosols into a narrow band radiative transfer model (*46*). These results were then subtracted from the $T_{6.7}$ computed using the control simulations of temperature and water vapor mixing ratio, and the difference was plotted in Fig. 3.
39. Because, the $T_{6.7}$ depends on both Planck emission (temperature) and atmospheric opacity (water vapor mass), variations in $T_{6.7}$ cannot be unambiguously related to changes in water vapor mass, but rather are largely determined by changes in relative humidity (*47*, *48*).
40. The "constant rh" $T_{6.7}$ was calculated as in (*38*), but replacing the model-predicted water vapor mixing ratio with that obtained by fixing the relative humidity to its seasonally varying climatological value. Thus as the atmosphere cools, the mixing ratio used to compute the $T_{6.7}$ decreases at a constant relative humidity rate.
41. The "no drying" $T_{6.7}$ was calculated as in (*38*), but replacing the model-predicted water vapor mixing ratio with its seasonally varying climatological value. Thus, as the atmosphere cools, the mixing ratio used to compute the $T_{6.7}$ remains unchanged.
42. We follow the same procedure as Hall and Manabe (*27*) in configuring the "no water vapor feedback" version of the GCM.
43. Santer *et al*. (*33*) provide three different estimates of the MSU lower tropospheric temperature (2LT) record, which differ according to the index used to remove the ENSO signal. The time-average, global-mean cooling for the three versions of their data are 0.29 K (Niño 3 index). 0.32 K (Niño 3.4 index), and 0.36 K (SOI index). Because our results are insensitive to which version is used, for clarity, we have plotted only the intermediate of the three versions (Niño 3,4 index) in Figs. 2 and 4.
44. B. Santer *et al*., *J. Geophys. Res.* **104**, 6305 (1999).
45. J. Bates, X. Wu, D. Jackson, *J. Clim.* **9**, 427 (1996).
46. B. Soden *et al*., *Bull. Am. Meteorol. Soc.* **81**, 797 (2000).
47. F. Moller, *Planet. Space Sci.* **5**, 202 (1963).
48. B. Soden, F. Bretherton, *J. Geophys. Res.* **98**, 16669 (1993).
49. We acknowledge contributions and assistance from I. Held, V. Ramaswamy, N. C. Lau, A. Hall, J. Bates, D. Randel, B. Santer, J. Susskind, and T. Von der Haar; and we thank S. Solomon for early discussions and encouragement that eventually led to this study. Partially supported by NASA grant NAG 5-9792, NSF grant ATM-9988419.

7 February 2002; accepted 19 March 2002

The North Atlantic Spring Phytoplankton Bloom and Sverdrup's Critical Depth Hypothesis

D. A. Siegel,[1]* S. C. Doney,[2] J. A. Yoder[3]

More than 50 years ago, Harald Sverdrup developed a simple model for the necessary conditions leading to the spring bloom of phytoplankton. Although this model has been used extensively across a variety of aquatic ecosystems, its application requires knowledge of community compensation irradiance (I_C), the light level where photosynthetic and ecosystem community loss processes balance. However, reported I_C values have varied by an order of magnitude. Here, I_C estimates are determined using satellite and hydrographic data sets consistent with the assumptions in Sverdrup's 1953 critical depth hypothesis. Retrieved values of I_C are approximately uniform throughout much of the North Atlantic with a mean value of 1.3 mol photons meter^{-2} day^{-1}. These community-based I_C determinations are roughly twice typical values found for phytoplankton alone indicating that phytoplankton account for approximately one-half of community ecosystem losses. This work also suggests that important aspects of heterotrophic community dynamics can be assessed using satellite observations.

The spring bloom of phytoplankton in the North Atlantic Ocean has long fascinated oceanographers from the 1930s to 1950s (*1*–*3*) to the present day, where large interdisciplinary field experiments have been conducted to assess its role in the global carbon cycle (*4*). When viewed from space, the North Atlantic spring bloom is among the largest mass greenings observed on the Earth surface extending over scales of more than 2000 km (*5*–*7*). The North Atlantic spring bloom propagates to the north at speeds of the order of 20 km day^{-1} as can be clearly seen in time series observations of chlorophyll pigment concentration (Chl) made from spaceborne sensors (*8*).

Sverdrup's 1953 critical depth hypothesis (*1*) has been applied to a variety of aquatic ecosystems in an effort to quantify the roles of light availability and vertical mixing leading to spring blooms of phyto-

[1]Institute for Computational Earth System Science and Department of Geography, University of California Santa Barbara, Santa Barbara, CA 93106–3060, USA. [2]National Center for Atmospheric Research, 1850 Table Mesa Drive, Boulder, CO 80305, USA. [3]Graduate School of Oceanography, University of Rhode Island, Narragansett, RI 02882–1197, USA.

*To whom correspondence should be addressed. E-mail: davey@icess.ucsb.edu